SCHWEIZ. MINERAL. PETROGR. MITT. 82, 537–547, 2002

Crystal chemistry and structure refinements of barian muscovites from the Berisal Complex, Simplon region, Switzerland

by *Thomas Armbruster*[1], *Peter Berlepsch*[1], *Edwin Gnos*[2] and *Callum J. Hetherington*[3]

Abstract

The structures of seven muscovite-2M_1 crystals from the Berisal Complex, with Ba between 0.04 and 0.35 pfu, were refined from single-crystal X-ray data. The crystal with the highest Ba content has the composition $(K_{0.49}Ba_{0.35}Na_{0.14})(Al_{1.77}Mg_{0.14}Fe_{0.06}Ti_{0.05})[Si_{2.82}Al_{1.18}O_{10}](OH)_2$, space group $C2/c$, $Z = 2$, $a = 5.198(1)$, $b = 9.017(3)$, $c = 19.895(5)$ Å, $\beta = 95.79(2)°$, $V = 927.7$ Å^3. Ba is incorporated into dioctahedral micas mainly by the substitution Ba + $^{[IV]}$Al ↔ K + $^{[IV]}$Si and to a lesser extent by Ba + $^{[VI]}$(Mg,Fe^{2+}) ↔ K + $^{[VI]}$Al. Both types of substitution cause a lateral expansion of the sheets, observed as an increase of the *a* and *b* cell dimensions. The distortions of tetrahedral and octahedral sheets are very similar to ordinary muscovites leading to tetrahedral rotations of $\alpha = 10.6$–$11.5°$ for both Ba-poor and barian muscovites. Because of the similar ionic radii of Ba^{2+} and K$^+$, all crystals investigated have I – O_{inner} average distances of 2.83 Å that is achieved by a reduction of the interlayer separation with increasing Ba content. Thus the lateral expansion, which would increase I – O_{inner}, is counterbalanced by decreasing the interlayer separation. Extrapolation to the hypothetical Ba end-member yields an interlayer separation of about 3.1 Å, very similar to paragonite, whereas muscovite has an interlayer separation of about 3.45 Å. The reduced interlayer separation in barian muscovites is also reflected in the lattice spacing perpendicular to (001), expressed by $c \times \sin\beta$, if a correction for the paragonite content (Na on I) is applied.

Keywords: Muscovite, crystal structure, Ba substitution, crystal chemistry.

Introduction

Complete Ba substitution for K (Ba + $^{[IV]}$Al ↔ K + $^{[IV]}$Si) in trioctahedral micas-1*M* (BRIGATTI and POPPI, 1993) leads to kinoshitalite $BaMg_3[Al_2Si_2O_{10}](OH)_2$ (e.g., GNOS and ARMBRUSTER, 2000). However, a corresponding complete Ba substituted end-member in dioctahedral micas-2*M* is unknown. To our knowledge the highest Ba concentration (12.9 wt% BaO) in dioctahedral micas was reported by DEVARAJU et al. (1999) from an Archean barite deposit in India leading to the formula $K_{0.45}Ba_{0.36}Na_{0.17}(Al_{1.78}Mg_{0.12}Ti_{0.05}Cr_{0.03})[Al_{1.18}Si_{2.82}O_{10}](OH)_2$. Additional studies on barian muscovites and phengites were reviewed by HARLOW (1995). HARLOW (1995) defined the Ba exchange reactions Ba + $^{[IV]}$Al ↔ K + $^{[IV]}$Si and Ba + $^{[VI]}$(Mg,Fe^{2+}) ↔ K + $^{[VI]}$Al as responsible for Ba incorporation in dioctahedral micas. Recently HETHERINGTON et al. (2000) published an abstract on the first barium-dominant muscovite type mica-2M_1 of average composition $Ba_{0.44}K_{0.26}Na_{0.28}(Al_{1.86}Mg_{0.08}Fe_{0.04}Ti_{0.03})[Al_{1.34}Si_{2.66}O_{10}](OH)_2$ from the Berisal Complex. Petrography and petrology of the corresponding barium-rich rocks have been discussed by FRANK (1979) and HETHERINGTON et al. (1999, 2000).

Chernykhite (ANKINOVICH et al., 1972; ROZHDESTVENSKAYA, 1979) with the simplified formula $(Ba,Na,\square)(V^{3+},Al,V^{4+})_2[Al_{1.7}Si_{2.3}O_{10}](OH)_2$ is another barium dominant dioctahedral mica-2M_1, although the interlayer position is only partially occupied (commonly less than 50%).

[1] Laboratorium für chemische und mineralogische Kristallographie, Universität Bern, Freiestr. 3, CH-3012 Bern. <thomas.armbruster@krist.unibe.ch>
[2] Institut für Geologie, Universität Bern, Baltzerstr. 1, CH-3012 Bern.
[3] Mineralogisch-petrographisches Institut, Universität Basel, Bernoullistr. 30, CH-4056 Basel
Present address: Geologisk Museum Universitetet Natuhistoriske Museer og Botanisk Hage, Postboks 1172, N-0318 Oslo, Norway.

This paper reports on crystal structure refinements of barian muscovites from the same rock samples of the Berisal Complex from which also Ba-dominant muscovite-2M_1 was described (HETHERINGTON et al., 2000). The highest Ba concentration in our dioctahedral micas, suitable for single-crystal structure analysis, was 0.35 Ba pfu, though considerably less than found for the Ba-dominant muscovite-2M_1 (HETHERINGTON et al., 2000). All formula units stated in this paper are normalized to 22 negative charges (11 oxygen atoms). Crystal structure refinements of barian muscovites have hitherto not been reported.

Experimental

SAMPLE DESCRIPTIONS

Seven (1+3+3) muscovite crystals were extracted from three different rock samples originating

Table 1 Electron microprobe analyses on seven Ba bearing muscovites for which also single-crystal X-ray data were collected. Analyses were normalized on 22 negative charges.

Crystal #	1	2	3	4	5	6	7
Analyses	4	4	5	5	5	5	5
K_2O	7.15(8)	5.89(50)	6.08(58)	5.34(59)	8.86(19)	8.63(9)	8.72(17)
BaO	8.12(10)	11.46(1.15)	9.94(1.79)	12.48(93)	1.49(17)	1.70(23)	1.79(31)
Na_2O	0.98(4)	0.95(4)	1.00(12)	1.03(18)	1.54(13)	1.57(13)	1.50(13)
CaO	0.01(1)	0.01(1)	0.01(1)	0.01(1)	0.01(1)	0.04(6)	0.03(3)
SiO_2	42.29(41)	41.20(59)	37.51(82)	39.51(65)	46.46(22)	46.44(27)	45.22(41)
Al_2O_3	33.82(24)	35.30(36)	35.07(1.10)	35.08(17)	36.10(18)	36.19(37)	35.74(14)
TiO_2	0.79(3)	0.93(12)	0.68(19)	0.85(9)	0.36(5)	0.31(7)	0.33(6)
Fe_2O_3	1.55(7)	1.28(9)	0.84(17)	1.15(7)	0.52(6)	0.51(4)	0.54(5)
MgO	1.59(1)	1.38(7)	0.77(25)	1.28(6)	0.98(8)	1.00(5)	0.90(10)
MnO	0.02(3)	0.02(3)	0.03(2)	0.01(3)	0.03(1)	0.02(2)	0.02(2)
F	0.14(11)	0.20(8)	0.08(8)	0.18(4)	0.08(3)	0.10(4)	0.12(7)
Cl	0.01(0)	0.00(0)	0.00(0)	0.00(0)	0.00(0)	0.01(1)	0.01(1)
Sum	96.47(56)	98.63(62)	92.01(42)	96.90(58)	96.44(36)	96.52(58)	94.93(29)
K	0.64(0)	0.53(4)	0.57(5)	0.49(5)	0.75(1)	0.73(1)	0.75(1)
Ba	0.22(0)	0.31(4)	0.29(6)	0.35(3)	0.04(1)	0.04(1)	0.05(1)
Na	0.13(0)	0.13(1)	0.14(2)	0.14(3)	0.20(2)	0.20(1)	0.20(2)
Ca	0.00(0)	0.00(0)	0.00(0)	0.00(0)	0.00(0)	0.00(0)	0.00(0)
Si	2.95(1)	2.87(3)	2.78(2)	2.82(3)	3.06(1)	3.06(2)	3.04(2)
Al	2.78(2)	2.90(4)	3.06(6)	2.95(2)	2.81(1)	2.81(2)	2.84(2)
Mg	0.17(1)	0.14(1)	0.08(3)	0.14(1)	0.10(1)	0.10(1)	0.09(1)
Fe	0.08(0)	0.07(1)	0.05(1)	0.06(1)	0.03(1)	0.03(0)	0.03(0)
Ti	0.04(0)	0.05(0)	0.04(1)	0.05(1)	0.02(0)	0.02(1)	0.02(1)
Mn	0.00(0)	0.00(0)	0.00(0)	0.00(0)	0.00(0)	0.00(0)	0.00(0)
F	0.03(2)	0.05(2)	0.02(2)	0.04(1)	0.02(1)	0.02(1)	0.03(2)
Cl	0.00(0)	0.00(0)	0.00(0)	0.00(0)	0.00(0)	0.00(0)	0.00(0)
O	11	11	11	11	11	11	11
Ba+Na+K	0.99(1)	0.97(1)	1.01(1)	0.98(2)	0.99(1)	0.97(2)	0.99(1)
$(Si+Al)^{IV}$	4	4	4	4	4	4	4
$(Al+Mg+Fe+Ti)^{VI}$	2.02(2)	2.02(1)	2.01(1)	2.02(1)	2.02(2)	2.02(1)	2.01(1)

Table 2 Selected structure refinement results and lattice parameters..

Sample	Dimensions [mm]	N_{obs} $I > 2\times\sigma_I$	R_{int} × 100	R_σ × 100	R_1 × 100	a [Å]	b [Å]	c [Å]	β [º]	V [Å^3]
1	.30 × .30 × .05	781	6.84	6.33	6.16	5.198(1)	9.018(3)	19.925(5)	95.78(2)	929.2
2	.15 × .05 × .05	807	1.70	2.90	3.11	5.202(1)	9.025(3)	19.925(7)	95.81(2)	930.6
3	.15 × .15 × .03	832	5.10	3.60	5.41	5.201(1)	9.023(3)	19.910(5)	95.84(2)	929.7
4	.20 × .10 × .03	769	4.85	13.77	4.14	5.198(1)	9.017(3)	19.895(5)	95.79(2)	927.7
5	.30 × .25 × .05	1050	1.53	1.85	2.44	5.178(1)	8.987(4)	19.946(5)	95.71(2)	923.7
6	.35 × .20 × .05	1108	1.35	2.24	2.11	5.1811(9)	8.987(1)	19.959(3)	95.71(1)	924.8
7	.25 × .18 × .05	883	2.36	4.34	2.80	5.1821(6)	8.993(1)	19.960(3)	95.74(1)	925.5

from the Berisal Complex, Simplon region, Switzerland. The muscovites are silvery-white in color, transparent and display the usual perfect (001) cleavage. The crystal habit is platy with a thickness ranging from about 0.03 to 0.05 mm and an edge length of the plates varying from 0.05 to 0.3 mm. The actual localities are all from a very small geographical area, but the assemblages differ. Crystals 1 to 4 are from two examples of white mica schist. The mineral assemblage is Ba-rich white mica, quartz, zoisite, zircon, and apatite. The two lenses of schist, from which the crystals were taken, are < 10 cm in thickness and outcrop in a larger body of zoisite-celsian gneiss, the source of crystals 5 to 7. The gneiss contains a metamorphic assemblage of zoisite, celsian, white mica, quartz, margarite, and rutile.

Table 3 Representative data collection and structure refinement parameters for two barian muscovites (#2 and #6).

Crystal	#2	#6
Diffractometer	Enraf Nonius CAD4	
X-ray radiation	Mo$K\alpha$	
X-ray power	50 kV, 40 mA	
Temperature	293 K	
Maximum 2θ	60°	
Measured reflections	1740	1728
Index range	$-7 \le h \le 7$	
	$-1 \le k \le 12$	
	$-1 \le l \le 27$	
Scan type	Omega	
Scan angle × 0.35 tanθ	4°	1.9°
Maximum scan time	120 s	120 s
Unique reflections > $2\sigma(I)$	807	1108
$R\sigma$	2.90	2.24
Number of l.s. parameters	92	91
GooF	1.140	1.127
$R_1, F_o > 4\sigma(F_o)$	3.06	2.06
R_1, all data	3.06	3.72
wR_2 (on F_o^2)	8.03	6.72

$R_{int} = \Sigma\, |F_o^2 - F_o^2\,(\text{mean})| \,/\, \Sigma\, F_o^2$
$R_\sigma = \Sigma\, \sigma(F_o^2) \,/\, \Sigma\, F_o^2$
$R_1 = \Sigma\, ||F_o| - |F_c|| \,/\, \Sigma\, |F_o|$
$wR_2 = \sqrt{(\Sigma\, w[F_o^2 - F_c^2]^2 \,/\, \Sigma\, w[F_o^2]^2)}$
Goof = $\sqrt{(\Sigma\, w[F_o^2 - F_c^2] \,/\, [n-p])}$
#2: $w = 1 / (\sigma^2[F_o^2] + [0.0327 * P]^2 + 9.1993 * P)$
#6: $w = 1 / (\sigma^2[F_o^2] + [0.0394 * P]^2 + 0.4145 * P)$
$P = (\text{Max}\,[F_o^2, 0] + 2 * F_c^2) / 3$

CHEMICAL ANALYSES

The seven muscovite crystals, used for X-ray data collection, were analyzed with a Cameca SX-50 electron microprobe (EMP) using beam conditions of 15 kV and 20 nA, wavelength-dispersive spectrometers, and an enlarged spot size of 15 µm to minimize damage of the hydrous minerals. The PAP procedure (Pouchou and Pichoir, 1984) was used for matrix correction. The following natural or synthetic standards were used: orthoclase (Si, K), albite (Na), anorthite (Ca, Al), almandine (Fe), spinel (Mg), tephroite (Mn), ilmenite (Ti), fluorphlogopite (F), scapolite (Cl), and barite (Ba). TiKα and BaLα were measured on a LiF crystal where the two lines are not overlapping, and benitoite was used as secondary standard. Data on peak and background for Ba, Ti, Cl and F were collected for 30 s, all other elements for 20 s. Note that mica cleavage flakes were analysed

Table 4 Formulae for barian muscovites obtained from chemical and structural analyses.

#		I	M	T	
1	a	$(K_{0.64(0)}Ba_{0.22(0)}Na_{0.13(0)})_{\Sigma=0.99(1)}$	$(Al_{1.73(2)}Mg_{0.17(1)}Fe_{0.08(0)}Ti_{0.04(0)})_{\Sigma=2.02(2)}$	$(Si_{2.95(1)}Al_{1.05(2)})_{\Sigma=4}$	$O_{10}(OH)_{1.97}F_{0.03(2)}$
	b	$(K_{0.66}Ba_{0.20}Na_{0.14})_{\Sigma=1}$	M: $Al_{2.00}$ M_T: $Fe_{0.03}$ $\Sigma = 2.03$	$(Si_{2.95}Al_{1.05})$	$O_{10}(OH)_2$
2	a	$(K_{0.53(4)}Ba_{0.31(4)}Na_{0.13(1)})_{\Sigma=0.97(1)}$	$(Al_{1.77(4)}Mg_{0.14(1)}Fe_{0.07(1)}Ti_{0.05(0)})_{\Sigma=2.02(1)}$	$(Si_{2.87(3)}Al_{1.13(4)})_{\Sigma=4}$	$O_{10}(OH)_{1.95}F_{0.05(2)}$
	b	$(K_{0.55}Ba_{0.32}Na_{0.13})_{\Sigma=1}$	M: $(Al_{1.96}Fe_{0.04})$ $\Sigma = 2$	$(Si_{2.87}Al_{1.13})$	$O_{10}(OH)_2$
3	a	$(K_{0.57(5)}Ba_{0.29(6)}Na_{0.14(2)})_{\Sigma=1.01(1)}$	$(Al_{1.84(6)}Mg_{0.08(3)}Fe_{0.05(1)}Ti_{0.04(1)})_{\Sigma=2.01(1)}$	$(Si_{2.78(2)}Al_{1.22(6)})_{\Sigma=4}$	$O_{10}(OH)_{1.98}F_{0.02(2)}$
	b	$(K_{0.55}Ba_{0.32}Na_{0.13})_{\Sigma=1}$	M: $(Al_{1.94}Fe_{0.06})$ $\Sigma = 2$	$(Si_{2.78}Al_{1.22})$	$O_{10}(OH)_2$
4	a	$(K_{0.49(5)}Ba_{0.35(3)}Na_{0.14(3)})_{\Sigma=0.98(2)}$	$(Al_{1.77(2)}Mg_{0.14(1)}Fe_{0.06(1)}Ti_{0.05(1)})_{\Sigma=2.02(1)}$	$(Si_{2.82(3)}Al_{1.18(2)})_{\Sigma=4}$	$O_{10}(OH)_{1.96}F_{0.04(1)}$
	b	$(K_{0.53}Ba_{0.32}Na_{0.15})_{\Sigma=1}$	M: $Al_{2.00}$ M_T: $Fe_{0.03}$ $\Sigma = 2.03$	$(Si_{2.82}Al_{1.18})$	$O_{10}(OH)_2$
5	a	$(K_{0.75(1)}Na_{0.20(2)}Ba_{0.04(1)})_{\Sigma=0.99(1)}$	$(Al_{1.87(1)}Mg_{0.10(1)}Fe_{0.03(1)}Ti_{0.02(0)})_{\Sigma=2.02(2)}$	$(Si_{3.06(1)}Al_{0.94(1)})_{\Sigma=4}$	$O_{10}(OH)_{1.98}F_{0.02(1)}$
	b	$(K_{0.75}Na_{0.20}Ba_{0.05})_{\Sigma=1}$	M: Al_2	$(Si_{3.06}Al_{0.94})$	$O_{10}(OH)_2$
6	a	$(K_{0.73(1)}Na_{0.20(1)}Ba_{0.04(1)})_{\Sigma=0.97(2)}$	$(Al_{1.87(1)}Mg_{0.10(1)}Fe_{0.03(0)}Ti_{0.02(1)})_{\Sigma=2.02(1)}$	$(Si_{3.06(2)}Al_{0.94(2)})_{\Sigma=4}$	$O_{10}(OH)_{1.98}F_{0.02(1)}$
	b	$(K_{0.74}Na_{0.20}Ba_{0.06})_{\Sigma=1}$	M: Al_2	$(Si_{3.06}Al_{0.94})$	$O_{10}(OH)_2$
7	a	$(K_{0.75(1)}Na_{0.20(2)}Ba_{0.05(1)})_{\Sigma=0.99(1)}$	$(Al_{1.88(2)}Mg_{0.09(1)}Fe_{0.03(0)}Ti_{0.02(1)})_{\Sigma=2.01(1)}$	$(Si_{3.04(2)}Al_{0.96(2)})_{\Sigma=4}$	$O_{10}(OH)_{1.97}F_{0.03(2)}$
	b	$(K_{0.74}Na_{0.20}Ba_{0.06})_{\Sigma=1}$	M: Al_2	$(Si_{3.04}Al_{0.96})$	$O_{10}(OH)_2$
Ga		$(Ba_{0.44}K_{0.26}Na_{0.28})_{\Sigma=0.98}$	$(Al_{1.86}Mg_{0.08}Fe_{0.04}Ti_{0.03})_{\Sigma=2.01}$	$(Si_{2.66}Al_{1.34})_{\Sigma=4}$	$O_{10}(OH)_2$

General formula: $IM_2T_4O_{10}(OH)_2$
a result from electron microprobe analyses
b result from crystal structure refinement
Ga composition of Ba dominant muscovite given by Hetherington et al. (2000)

without previous polish. Results of the EMP analyses are summarized in Table 1.

X-RAY DATA COLLECTION AND STRUCTURE REFINEMENT

Single-crystal X-ray data collections on the same seven crystals used for chemical analysis were performed with an ENRAF NONIUS CAD4 single-crystal X-ray diffractometer using graphite monochromated Mo$K\alpha$ X-radiation. Cell dimensions were refined from 22 reflections with high θ angles yielding monoclinic symmetry and the cell parameters listed in Table 2. All crystals are $2M_1$ polytypes. Experimental details for two representative structure refinements (crystals 2 and 6) are given in Table 3. Diffraction data were collected up to θ = 30°. Data reduction, including background and Lorentz polarization correction, was carried out with the SDP program system (ENRAF NONIUS, 1983). An empirical absorption correction using the Ψ-scan technique was routinely applied. However, anisotropy of absorption was not a major problem as evidenced by relative transmission factors varying between ca. 0.83 and 0.98 for all crystals. Systematic absences confirmed *C*2/*c* as the correct space group for the studied $2M_1$ polytypes. In particular, the Ba-rich crystals exhibited pronounced smearing of reflections perpendicular to c* requiring extended omega scans for data collection (Table 3).

The structure of barian muscovite-$2M_1$ was solved with the program SHELXS-97 (SHELDRICK, 1997) and refined with the program SHELXL-97 applying neutral atom scattering factors (SHELDRICK, 1997). Refinement of the I-site population was guided by the EMP analyses (Table 1): the Ba content was refined against a hypothetical element representing the analyzed K/Na ratio (in terms of electrons) and the sum was constrained to full occupancy. Subsequently the site occupancy factor of the hypothetical element was decomposed into K and Na values. Si and Al scattering curves, according to the EMP analyses, were assigned to the tetrahedral T-sites. Populations of octahedral M-sites were refined allowing for Al (modeling Al and Mg) and Fe

Table 5 Fractional atomic coordinates, isotropic displacement parameters (Å^2) and site occupancy factors (sof) for structure refinements of crystals #2 and 6.

Crystal #2: $K_{0.53}Ba_{0.31}Na_{0.13})(Al_{1.77}Mg_{0.14}Fe_{0.07}Ti_{0.05})[Si_{2.87}Al_{1.13}O_{10}](OH)_2$						
Label	Type	*x*/*a*	*y*/*b*	*z*/*c*	U_{iso}	sof
IA	Ba	0	0.90081(12)	0.25	0.0186(3)	0.318(4)
IB	Na,K	0	0.90081(12)	0.25	0.0186(3)	0.682(4)
T1	Si	0.0350(3)	0.57045(15)	0.36344(7)	0.0094(3)	1
T2	Si	0.0480(2)	0.24144(18)	0.36362(7)	0.0094(3)	1
MA	Al	0.7495(3)	0.58316(16)	0.50002(7)	0.0075(4)	0.986(6)
MB	Fe	0.7495(3)	0.58316(16)	0.50002(7)	0.0075(4)	0.014(6)
O1	O	0.2500(7)	0.1303(4)	0.32911(18)	0.0164(8)	1
O2	O	0.5813(7)	0.9071(4)	0.32959(16)	0.0165(7)	1
O3	O	0.1134(6)	0.2487(4)	0.44616(17)	0.0137(7)	1
O4	O	0.2488(7)	0.6888(4)	0.33974(18)	0.0188(8)	1
O5	O	0.0395(7)	0.5564(4)	0.44632(17)	0.0121(7)	1
O6	O	0.4576(7)	0.5613(4)	0.55131(18)	0.0142(8)	1
H6	H	0.389(15)	0.643(8)	0.553(4)	0.05	1
Crystal #6: $K_{0.73}Na_{0.20}Ba_{0.06})(Al_{1.87}Mg_{0.10}Fe_{0.03}Ti_{0.02})[Si_{3.06}Al_{0.94}O_{10}](OH)_2$						
Label	Type	*x*/*a*	*y*/*b*	*z*/*c*	U_{iso}	sof
IA	Ba	0	0.90121(6)	0.25	0.0238(2)	0.0495(15)
IB	Na,K	0	0.90121(6)	0.25	0.0238(2)	0.9505(15)
T1	Si	0.03529(8)	0.57031(5)	0.36406(2)	0.00834(11)	1
T2	Si	0.04875(8)	0.24147(5)	0.36400(2)	0.00833(11)	1
M	Al	0.74968(8)	0.58332(5)	0.50003(2)	0.00787(11)	1
O1	O	0.2493(2)	0.12874(14)	0.33027(6)	0.0156(2)	1
O2	O	0.5858(2)	0.90705(12)	0.33092(6)	0.0157(2)	1
O3	O	0.1157(2)	0.24851(11)	0.44637(5)	0.0107(2)	1
O4	O	0.2491(2)	0.69042(14)	0.34175(6)	0.0172(2)	1
O5	O	0.0381(2)	0.55605(12)	0.44634(5)	0.0107(2)	1
O6	O	0.4576(2)	0.56144(13)	0.55049(5)	0.0118(2)	1
H6	H	0.390(6)	0.638(3)	0.5583(16)	0.05	1

(modeling Fe and Ti). If significant electron density was found on the larger M_T site (characteristic of trioctahedral micas) Fe was assigned. The H position, extracted from difference Fourier maps, was refined with the distance restrain O6 – H6 = 0.9(1) Å. Anisotropic displacement parameters were refined for all atoms in the last cycles except for the weakly populated trioctahedral M_T site (at ¼, ¾, ½) as well as the H site. The refinement was stopped when the maximum shift/estimated standard deviation (esd) for varied parameters dropped below 0.01. The refinement results for crystals 2 and 6 are represented in Tables 4 to 6. Corresponding coordinates and displacement parameters of the other crystals can be obtained from the senior author upon request.

Table 6 Anisotropic displacement parameters (Å²) for structure refinements of crystals #2 and 6.

Crystal #2: $(K_{0.53}Ba_{0.31}Na_{0.13})(Al_{1.77}Mg_{0.14}Fe_{0.07}Ti_{0.05})[Si_{2.87}Al_{1.13}O_{10}](OH)_2$						
Label	U_{11}	U_{22}	U_{33}	U_{23}	U_{13}	U_{12}
I	0.0193(5)	0.0194(5)	0.0170(5)	0	0.0013(3)	0
T1	0.0086(6)	0.0111(7)	0.0084(6)	0.0006(5)	0.0011(5)	0.0003(5)
T2	0.0089(6)	0.0105(6)	0.0087(6)	–0.0001(5)	0.0001(5)	–0.0001(5)
M	0.0064(6)	0.0088(6)	0.0073(6)	0.0010(5)	0.0001(4)	–0.0007(5)
O1	0.0153(17)	0.0191(19)	0.0144(16)	–0.0017(14)	0.0004(13)	0.0052(14)
O2	0.0219(17)	0.0160(16)	0.0116(15)	0.0013(15)	0.0014(13)	0.0015(16)
O3	0.0152(16)	0.0156(16)	0.0104(15)	0.0016(14)	0.0011(12)	–0.0022(15)
O4	0.0161(18)	0.023(2)	0.0161(18)	0.0038(16)	–0.0013(14)	–0.0052(16)
O5	0.0095(15)	0.0134(17)	0.0133(16)	–0.0006(13)	0.0012(12)	–0.0005(13)
O6	0.0172(17)	0.0110(18)	0.0150(17)	–0.0016(13)	0.0045(14)	0.0027(13)
Crystal #6: $(K_{0.73}Na_{0.20}Ba_{0.06})(Al_{1.87}Mg_{0.10}Fe_{0.03}Ti_{0.02})[Si_{3.06}Al_{0.94}O_{10}](OH)_2$						
Label	U_{11}	U_{22}	U_{33}	U_{23}	U_{13}	U_{12}
I	0.0254(3)	0.0244(3)	0.0214(3)	0	0.0021(2)	0
T1	0.0080(2)	0.00714(19)	0.0098(2)	0.00037(13)	0.00079(13)	0.00031(14)
T2	0.0078(2)	0.00736(19)	0.0097(2)	0.00018(13)	0.00054(14)	0.00031(14)
M	0.0073(2)	0.0067(2)	0.0096(2)	0.00064(14)	0.00050(15)	–0.00012(14)
O1	0.0152(5)	0.0179(6)	0.0143(5)	–0.0007(4)	0.0007(4)	0.0037(4)
O2	0.0219(6)	0.0110(5)	0.0143(5)	0.0005(4)	0.0025(4)	0.0019(4)
O3	0.0117(5)	0.0090(5)	0.0114(5)	0.0002(4)	0.0001(4)	–0.0003(4)
O4	0.0140(5)	0.0198(6)	0.0172(6)	0.0042(4)	–0.0007(4)	–0.0035(4)
O5	0.0097(5)	0.0109(5)	0.0116(5)	0.0009(4)	0.0012(4)	0.0006(4)
O6	0.0107(5)	0.0106(5)	0.0144(5)	–0.0022(4)	0.0026(4)	–0.0005(4)

Table 7 Parameters (BAILEY, 1984) describing the distortion of the tetrahedral and octahedral sheets in micas.

Crystal	α_{tet}	τ_{tet}	Ψ_{oct}	h_{tet}	h_{oct}	IS	Δz	T-O	M-O	I-O
1	10.61	111.6	57.0	2.245	2.106	3.294	0.220	1.646	1.933	2.847
		111.6	62.0					1.647	2.244	3.325
2	10.96	111.6	57.1	2.250	2.099	3.283	0.222	1.654	1.933	2.833
		111.7	62.2					1.652	2.249	3.334
3	10.94	111.8	57.1	2.250	2.099	3.274	0.221	1.652	1.934	2.831
		111.7	62.2					1.653	2.248	3.330
4	11.10	111.7	57.2	2.247	2.102	3.273	0.200	1.654	1.938	2.828
		111.7	62.0					1.651	2.240	3.332
5	11.64	111.1	57.2	2.221	2.085	3.340	0.206	1.644	1.923	2.827
		111.1	62.3					1.644	2.244	3.355
6	11.51	111.0	57.2	2.225	2.089	3.349	0.206	1.648	1.928	2.837
		111.0	62.3					1.647	2.245	3.354
7	11.53	111.2	57.1	2.227	2.089	3.345	0.210	1.645	1.924	2.831
		111.1	62.4					1.645	2.254	3.354

α: tetrahedral rotation (°); τ_{tet}: average angle $O_{apical} - T - O_{basal}$ (°); Ψ_{oct}: flattening angle (°) (ideal 54.44°); h_{tet}: tetrahedral thickness (Å); h_{oct}: octahedral thickness (Å); IS: interlayer separation (Å); Δz: tetrahedral height difference (Å); T-O: average T1-O and T2-O bond lengths (Å); M-O: average M-O (2×) and M_T-O (empty) bond lengths (Å); I-O: average I-O_{inner} and I-O_{outer} distances (Å).

Results

The chemical compostions of the seven muscovites, obtained from EMP analyses and structure refinements, are compared in Table 4. The results show an excellent agreement between the chemically analyzed and structurally refined Ba contents. Average T-O bond distances (Table 7) show no indication of Si, Al order between T1 and T2 which agrees with the results on Fe^{2+}, Mg-bearing muscovites studied by BRIGATTI et al. (1998). In the case of crystals 2 and 3 some Fe was localized on the M site and thus Σ (Al+Fe) = 2 apfu. Partial occupation of trioctahedral M_T was observed in crystals 1 and 4 (occupancy 0.60 and 0.79 electrons, respectively), leading to a sum of M-site cations greater than 2 (Table 4). Similar low occupancies for this site were reported by BRIGATTI et al. (1998). In crystal 4 a low populated (0.52 electrons) additional interlayer site at 0.582(7), 0.108(4), 0.255(2) was found probably indicating either the presence of a very minor additional polytype or substantial stacking faults.

All crystals investigated show a significant paragonite component with Na concentrations between 0.13 and 0.20 Na pfu. Ba concentrations range from 0.05 to 0.35 pfu. In addition, the concentration of larger cations (relative to Al) in octahedral coordination (Σ[Mg + Fe + Ti]) varies between 0.14 and 0.29 pfu. The cell volume of the crystals varies between 923.7 and 930.6 Å^3 (Table 2). Notice that a muscovite-2*M* with near end-member composition has a cell volume of about 935 Å^3 (GUIDOTTI, 1984). Thus the observed decreased volumes are mainly related to the paragonite content. Paragonite-2*M* with near end-member composition has a cell volume of about 880 Å^3 (LIN and BAILEY, 1984; COMODI and ZANAZZI, 1997).

Discussion

BUILDING PRINCIPLES OF DIOCTAHEDRAL MICAS

The fundamental problems of mica crystal-chemistry were reviewed by BAILEY (1984) and GUGGENHEIM (1984). The lateral extent of a dioctahedral Al sheet leads, for a *C*-centered setting, to $b = 8.655$ Å, the average found for gibbsite and bayerite $Al(OH)_3$. In contrast, a fully extended tetrahedral sheet $[Si_3AlO_{10}]^{5-}$ composed of ideal tetrahedra with random Si, Al distribution has a corresponding dimension of $b = 9.33$ Å (BAILEY, 1984). In order to have a stable junction at the octahedral-tetrahedral interface the lateral dimension of the sheets must be similar. The *b*-dimension of the tetrahedral sheet can be reduced by rotating adjacent tetrahedra in opposite direction in the (001) plane. The amount of rotation necessary to relieve

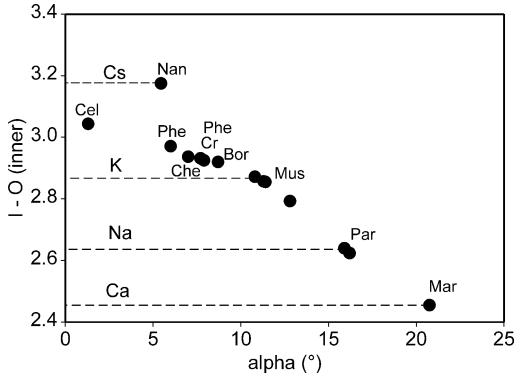

Fig. 1 Observed tetrahedral α rotations angles (explained in the text) for dioctahedral micas plotted versus the mean $I - O_{inner}$ distance (Å). Muscovite (Mus), phengite (Phe), paragonite (Par), chernykhite (Che) data are listed in BAILEY (1984), margarite (Mar) by GUGGENHEIM (1984); Nanpingite (Nan): NI and HUGHES (1996); Chromphyllite (Cr): EVSYUNIN et al. (1997); Boromuscovite (Bor): LIANG et al. (1995); Celadonite (Cel): ZHUKHLISTOV et al. (1977). Dashed horizontal lines indicate characteristic $I - O_{inner}$ distances for various cations on the interlayer site.

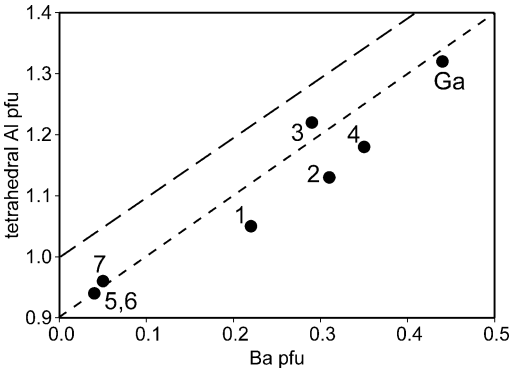

Fig. 2 Ba pfu (normalized to 22 negative charges) plotted versus tetrahedral Al pfu. The upper dashed line represents the substitution Ba + $^{[IV]}$Al ↔ K + $^{[IV]}$Si starting from stoichiometric muscovite $KAl_2[Si_3AlO_{10}](OH)_2$. The lower dashed line represents the same substitution offset by –0.1 $^{[IV]}$Al, equivalent with a phengite substitution (0.1 apfu) $^{[VI]}$Mg + $^{[IV]}$Si → $^{[VI]}$Al + $^{[IV]}$Al. All data points plot around this second line; crystal numbers are given in Table 1, Ga is the Ba dominant muscovite reported by HETHERINGTON et al. (2000).

the misfit is given by $\cos\alpha = b(\text{obs})/b(\text{ideal})$ where α is the rotation angle and b(ideal) is defined as the calculated b value of the fully extended tetrahedral sheet (BAILEY, 1984). The Al occupied dioctahedral sheet in micas has b = 9.0 Å, considerably larger than in $Al(OH)_3$ polymorphs due to specific polyhedral distortions (e.g., octahedral flattening). To fit a tetrahedral sheet $[Si_3AlO_{10}]^{5-}$ to an octahedral sheet with b = 9.0 Å a rotation angle of $\alpha = 15.2°$ is necessary. One of the consequences of the tetrahedral rotation is a deformation of the six-membered tetrahedral rings from hexagonal to trigonal symmetry leading to three short ($I - O_{inner}$) and three long distances ($I - O_{outer}$) to the interlayer cation (I). The $I - O_{inner}$ distances of various dioctahedral mica structures from the literature are plotted versus the rotation angle α in Fig. 1. A tetrahedral rotation of ca. 15° is realized for paragonite with Na on I. In order to fit the size of the tetrahedral rings to larger cations (e.g., K, Cs) a compromise becomes necessary; α decreases from 15° to increase $I - O_{inner}$ and additional tetrahedral and octahedral distortions operate to fit the tetrahedral sheet to the octahedral one. Margarite with Ca on I has a tetrahedral sheet of $[Si_2Al_2O_{10}]^{6-}$ composition (b_{ideal} = 9.52 Å) leading to a calculated α of 19°. In fact, the observed α angles for margarites are slightly above 20°. An additional way to adopt I – O distances which are in agreement with the ionic size is a variation of the interlayer separation leading to a range of $c \times \sin\beta$ values (NI and HUGHES, 1996). Thus a strict correlation between α and $I - O_{inner}$ cannot be expected (Fig. 1). The largest cation observed on I is Cs, and nanpingite $CsAl_2[Si_3AlO_{10}](OH)_2$ also exhibits the largest $c \times \sin\beta$ value of all dioctahedral 2M polytypes (NI and HUGHES, 1996).

Muscovites exhibit α rotations between about 10 and 13°. Boromuscovite (LIANG et al., 1995) has a smaller tetrahedral sheet of $[Si_{3.1}B_{0.68}Al_{0.22}O_{10}]^{4.9-}$ composition that reduces α to 8.7°. Smaller α rotations are also observed for dioctahedral micas with K on I where the octahedral sheet is partially occupied by larger cations (e.g., Mg, Fe^{2+} in phengite, Fe^{2+}, Fe^{3+} in celadonite, Cr^{3+} in chromphyllite, and V^{3+}, V^{4+} in chernykhite). A systematic structural study of muscovites-2M_1 with different degree of phengitic substitution has been performed by BRIGATTI et al. (1998).

An additional type of distortion, characteristic of the tetrahedral sheet in dioctahedral micas, is tetrahedral tilt leading to a basal-surface corrugation (BAILEY, 1984). This means that the exposed basal surface of the tetrahedral sheet is not flat but one bridging oxygen (O4 in this study) has a different height compared to the other basal oxygen atoms (O1 and O2 in this study). This height difference is expressed in the parameter Δz and is about 0.2 Å in muscovites.

BARIAN MUSCOVITES

In trioctahedral micas Ba favours two slightly different coordinations as exemplified in kinoshitalite $BaMg_3[Si_2Al_2O_{10}](OH)_2$ (GNOS and ARMBRUSTER, 2001) and anandite $BaFe_3[Si_3FeO_{10}](OH)S$ (FILUT et al., 1985). Kinoshitalite exhibits a very strong tetrahedral rotation with $\alpha = 17.9°$ leading to $Ba - O_{inner}$ = 2.837 Å and $Ba - O_{outer}$ = 3.396 Å. In contrast, anandite has $\alpha = 0.9°$ leading to $Ba - O_{inner}$ = 3.054 Å and $Ba - O_{outer}$ = 3.228 Å. This information and inspection of Fig. 1 suggest that a compound $BaAl_2[Si_2Al_2O_{10}](OH)_2$, analogous to margarite $CaAl_2[Si_2Al_2O_{10}](OH)_2$, probably does not exist. The hypothetic barium dioctahedral mica has a calculated tetrahedral rotation of $\alpha \approx 19°$ to fit the tetrahedral sheet to the octahedral one. Thus $Ba - O_{inner}$ distances in the range between 2.84 and 3.05 Å cannot be accomplished (Fig. 1). For barian muscovites we thus expect (1) tetrahedral rotations similar to muscovite and phengite of a 7–12° in order to provide an appropriate coordination for Ba, (2) either $Si >> {}^{[IV]}Al$ to reduce the size of the tetrahedral sheet and/or large trivalent cations (Fe^{3+}, Cr^{3+}, V^{3+}) in the dioctahedral sheet to reduce the sheet misfit, and (3) divalent cations in the dioctahedral sheet either according to a phengite substitution ${}^{[VI]}Mg + {}^{[IV]}Si \rightarrow {}^{[VI]}Al + {}^{[IV]}Al$ or according to $Ba + {}^{[VI]}(Mg, Fe^{2+}) \leftrightarrow K + {}^{[VI]}Al$ for balance of excess charge due to Ba on I. Divalent cations (Mg, Fe^{2+}) in the dioctahedral sheet lead also to an increase of its lateral extension. Note that the phengite substitution has the additional advantage of increasing the $Si/{}^{[IV]}Al$ ratio as suggested under (2).

As already suggested by HARLOW (1995) the substitutions (1) $Ba + {}^{[IV]}Al \leftrightarrow K + {}^{[IV]}Si$ and (2) $Ba + {}^{[VI]}(Mg,Fe^{2+}) \leftrightarrow K + {}^{[VI]}Al$ are the most important exchange reactions responsible for the varying Ba content in dioctahedral micas. In Figure 2 the Ba concentration is plotted versus the tetrahedral Al concentration and a dashed line is added representing the substitution $Ba + {}^{[IV]}Al \leftrightarrow K + {}^{[IV]}Si$ starting from stoichiometric muscovite $KAl_2[Si_3AlO_{10}](OH)_2$. A second dashed line represents the same substitution but is offset by –0.1 ${}^{[IV]}Al$, allowing for a phengite substitution (0.1 apfu) ${}^{[VI]}Mg + {}^{[IV]}Si \rightarrow {}^{[VI]}Al + {}^{[IV]}Al$. All data points plot around this second line. The horizontal deviation of the data points from the short-dashed line is defined as excess Ba due to a second substitution mechanism $Ba + {}^{[VI]}Mg \leftrightarrow K +$

$^{[VI]}$Al. Notice that excess Ba may also be negative for points above the line. Excess Ba is plotted versus Mg pfu in Fig. 3, and a dashed line is added representing the expected trend for a 0.1 apfu phengite substitution. Figures 2 and 3 indicate that the substitution Ba + $^{[VI]}$Mg ↔ K + $^{[VI]}$Al plays only a minor role for Ba incorporation. The influence of possible Fe^{2+} has been ignored because Fe^{2+} mainly balances Ti^{4+} and the valence of minor excess Fe cannot be calculated with certainty.

Another peculiarity of barian muscovites is the relatively short *c* cell dimension. End-member muscovite has *c* = 20.1 Å (GUIDOTTI, 1984) but the barian samples investigated in this study have *c* = 19.90 –19.93 Å. A better way to analyze this effect is the lattice spacing perpendicular to (001) expressed by $c \times \sin\beta$. This latter value also depends on the paragonite component (Na on I). GUIDOTTI (1984) derived the relationship $c \times \sin\beta = 2 \times (10 - 0.00217\ X - 0.0000259\ X^2)$ where X is Na % on I. This equation was used to correct the observed $c \times \sin\beta$ values for the paragonite component. $\Delta = (c \times \sin\beta)_{observed} - (c \times \sin\beta)_{predicted}$ is plotted versus analyzed Ba pfu (Fig. 4). The results indicate that $c \times \sin\beta$ decreases with increasing Ba concentration. The thickness of the tetrahedral and octahedral sheets (Table 7) are in

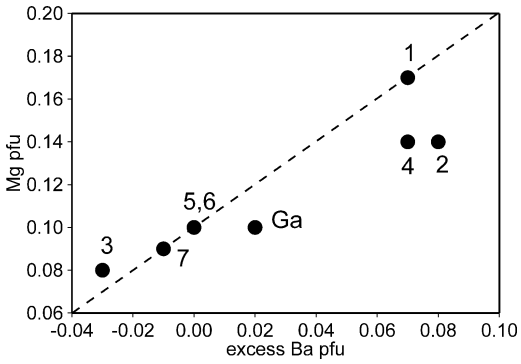

Fig. 3 Mg pfu (normalized to 22 negative charges) of samples from Table 1 is plotted versus the excess Ba content that is not charge balanced by the Ba + $^{[IV]}$Al ↔ K + $^{[IV]}$Si substitution but by Ba + $^{[VI]}$Mg ↔ K + $^{[VI]}$Al. Ga is the Ba dominant muscovite reported by HETHERINGTON et al. (2000). Excess Ba is calculated as Ba pfu + 0.9 – $^{[IV]}$Al. The dashed line represents the expected trend for a 0.1 apfu phengite substitution. Notice that the horizontal deviation (excess Ba) of samples 2 and 4 from the dashed line corresponds to 1 esd of analyzed Ba pfu listed in Table 1.

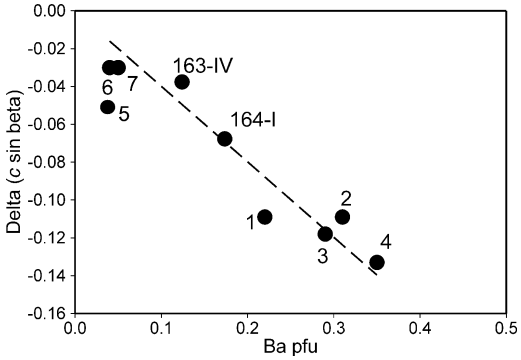

Fig. 4 Ba pfu of samples from Table 1, and 163-IV and 164-I from RAASE et al. (1983) is plotted versus $\Delta = (c \times \sin\beta)_{observed} - (c \times \sin\beta)_{predicted}$. The predicted values are corrected for the paragonite component in muscovites according to GUIDOTTI (1984). Note that the regression line is forced through the origin.

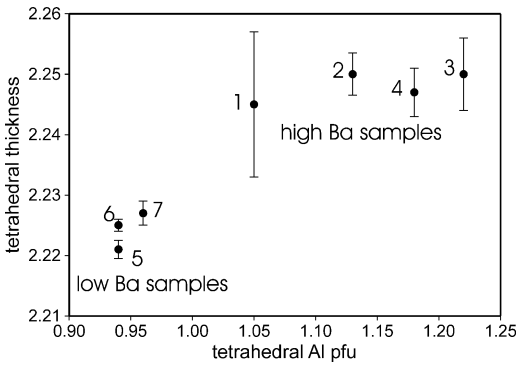

Fig. 5 Influence of the tetrahedral Al concentration on the thickness of the tetrahedral sheet. Note that tetrahedral Al is correlated with Ba pfu (Fig. 2). Error bars represent 2 estimated standard deviations (esd's).

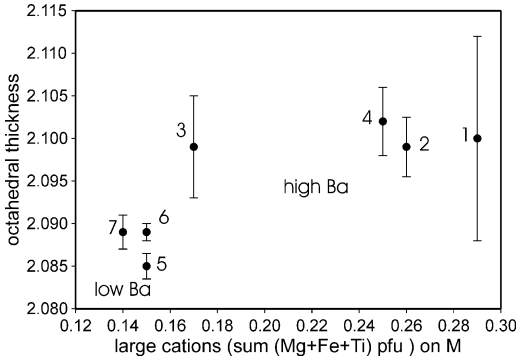

Fig. 6 Influence of large cations occupying the octahedral site on the thickness of the dioctahedral sheet. Error bars represent 2 estimated standard deviation.

agreement with values found for various muscovites (BAILEY, 1984) although there is a slight increase of both the tetrahedral and the octahedral thickness in the barian muscovites compared to our Ba-poor samples (Table 7). The increase in the tetrahedral thickness is related to the amount of tetrahedral Al (Fig. 5) and the increase in octahedral thickness is due to an increase of Σ (Mg + Fe + Ti) on M (Fig. 6). The basal surface corrugation of the tetrahedral sheet in barian muscovites (Δz = 0.20–0.21 Å) is also similar to our Ba-poor samples (Δz = 0.22 Å). The tetrahedral rotation angle α is about 11.5° for the Ba-poor samples and only slightly reduced (10.6–11.1°) for the barian muscovites (Table 7) which would increase $I - O_{inner}$.

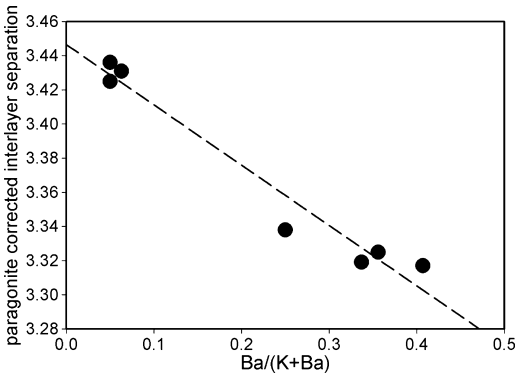

Fig. 7 Influence of Ba/(K+Ba) on the interlayer separation (IS) corrected for the effect of Na (paragonite). The dashed line represents a linear regression through the data points: IS (Å) = 3.446 – 0.3531 × Ba/(K+Ba), (r^2 = 0.958).

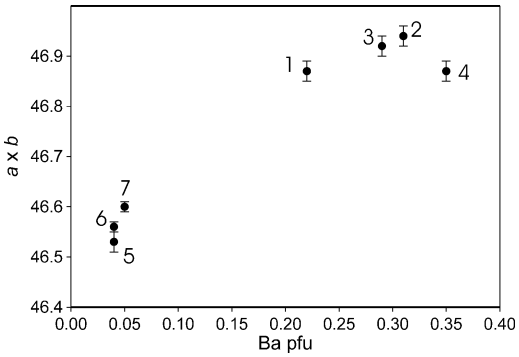

Fig. 8 Ba^{2+} in dioctahedral micas is mainly charge balanced by the substitutions Ba + $^{[IV]}$Al ↔ K + $^{[IV]}$Si and Ba + $^{[VI]}$(Mg,Fe^{2+}) ↔ K + $^{[VI]}$Al. Both types of substitution cause a lateral expansion of the sheets, observed as an increase of the *a* and *b* cell dimensions. The (001) surface area is determined by $a \times b$ (Å^2).

Reduced α for Ba rich muscovites decreases also $I - O_{outer}$ (Table 7) so that Ba^{2+} is more strongly coordinated helping to distribute its charge. This means that the decreased (001) basal spacing for barian muscovites must be related to a reduction of the interlayer separation because the $I - O_{inner}$ distances (2.83 Å) remain rather constant for all investigated crystals independent of their Ba concentration (Table 7). However, the interlayer separation ($IS = 2 \times c \times \sin\beta \times ((z_{O1} + z_{O2} + z_{O4})/3 - 0.25)$) is also dependent on the paragonite component thus a corresponding correction has to be applied assuming an interlayer separation (IS) of about 3.0 Å for end-member paragonite (BAILEY, 1984). The correction was done by determining $IS_{K,Ba} = (IS_{obs} - Na\ pfu \times 3.0)/(K + Ba)$. A plot of Na corrected interlayer separation (Fig. 7) versus Ba/(K+Ba) indicates a highly significant decrease with Ba content. A linear regression yields IS (Å) = 3.446 – 0.3531 × Ba pfu (r^2 = 0.958) and extrapolation to a hypothetical Ba end-member gives IS = 3.1 Å, almost identical to IS in paragonite (BAILEY, 1984). The similarity of sheet distortion-parameters (Table 7) for Ba-poor and Ba-rich dioctahedral micas supports a view that the size adoption of the tetrahedral sheet to fit the dioctahedral sheet in barian muscovites operates the same way as in normal muscovites (BRIGATTI et al., 1998) and that the bonding properties of Ba are accomplished by a characteristic decrease of the interlayer separation. As shown in Figs. 2 and 3, Ba is charge balanced by tetrahedral Al (replacing Si) and octahedral Mg (replacing Al). Both substitutions increase the lateral extension (Fig. 8) of the octahedral and tetrahedral sheets as evidenced by an increase of *a* and *b* cell dimensions with Ba content. Furthermore, there are additional effects such as the minor reduction of α for Ba-rich crystals. In total, these effects sum up and without compensation the $I - O_{inner}$ distance would increase with increasing Ba-content. Therefore, the decrease of the interlayer separation with Ba content counteracts the lateral expansion. K^+ in six-fold coordination has an ionic radius of 1.38 Å whereas the corresponding ionic radius of Ba^{2+} is 1.35 Å (SHANNON, 1976). The higher charge on Ba further strengthens the Ba–O bonds and makes them less 'flexible' than K–O bonds. Table 2 indicates that the unit cell volume slightly increases with Ba content. This means that the lateral extension of the mica structure, due to the Ba^{2+} charge balancing substitutions (octahedral Mg^{2+}, tetrahedral Al^{3+}), has a stronger effect on the volume than the decrease of $c \times \sin\beta$ with increasing Ba.

The variable IS to accommodate Ba was not foreseen in the predictions made above for barian

muscovites. However, a rough estimate shows that for the hypothetic end-member $BaAl_2[Si_2Al_2O_{10}](OH)_2$ with $\alpha \approx 19°$ an interlayer separation of ca. 4 Å would be required to obtain $I - O_{inner}$ of ca. 2.83 Å. An IS of 3.997 Å has also been determined for the Cs dioctahedral mica, nanpingite-$2M_2$ (NI and HUGHES, 1996). However, nanpingite has $\alpha = 5.45°$ and the tetrahedral sheet is almost fully expanded thus Cs is coordinated by twelve basal O atoms ($I - O_{inner} \approx I - O_{outer}$). Ba in hypothetical $BaAl_2[Si_2Al_2O_{10}](OH)_2$ would be six-coordinated ($I - O_{inner} >> I - O_{outer}$) and three closely spaced basal O atoms would sit above and below Ba. This coordination is highly unfavorable because the charge of Ba^{2+} is only vertically but not laterally shielded.

If one attempts to compare the structural findings for Berisal Complex barian muscovites, as discussed above, with barian muscovites from other occurrences a lack of information becomes evident. Although there exist several studies reporting Ba-enriched muscovites with Ba concentrations above 0.2 Ba pfu, only one study reports cell dimensions (RAASE et al., 1983) and only DYMEK et al. (1983), PAN and FLEET (1991), and HARLOW (1994) report the polytype ($2M_1$). Two data points of Ba-rich muscovites by RAASE et al. (1983) are added to Fig. 4, corroborating the decrease of $c \times \sin\beta$ with increasing Ba. If the available sets of chemical data are used to plot Ba pfu versus $^{[IV]}$Al (Figs. 2 and 9) it is evident that there is a general trend in each data set that Ba correlates with $^{[IV]}$Al but in addition a strong tendency of a phengite substitution $^{[VI]}(Mg, Fe^{2+}) + {}^{[IV]}Si \rightarrow {}^{[VI]}Al + {}^{[IV]}Al$ (independent of Ba) can be observed leading to a lateral extension of the dioctahedral sheet. For this reason DEVARAJU et al. (1999) postulated $Ba(Mg,Fe)Al[Si_3AlO_{10}](OH)_2$ as a possible end-member composition for a barium dioctahedral mica. Only the barian muscovites reported by TRACY (1991) lack a pronounced phengite substitution but these samples are very rich in interlayer Na and one may speculate that the similar interlayer separation for Ba and Na stabilizes Ba in muscovites. Nevertheless, there is no correlation between Ba and Na in this data set. Another potential candidate of the dioctahedral micas for Ba incorporation is chromphyllite $KCr_2[Si_3AlO_{10}](OH)_2$ (EVSYUNIN et al., 1997). The type material contained 0.14 Ba pfu and several barian-chromian muscovites were described (DYMEK et al. 1983; RAASE et al., 1983; PAN and FLEET, 1991). Chromphyllite and chernykhite $(Ba,Na,\square)(V^{3+},Al,V^{4+})_2[Al_{1.7}Si_{2.3}O_{10}](OH)_2$ (ANKINOVICH et al., 1972; ROZHDESTVENSKAYA, 1979) have the advantage of a larger lateral extension of the octahedral sheet ($b_{chromph.} = 9.10$ Å, $b_{cherny.} = 9.18$ Å) requiring lower α rotation angles of the tetrahedral sheet (Fig. 1). Lower α rotation angles in dioctahedral micas provide a more comfortable coordination for large (Ba) interlayer cations by shortening the $I - O_{outer}$ distance.

Therefore, the reason why certain compositions of dioctahedral micas are able to accommodate significant Ba is probably a reduced octahedral – tetrahedral sheet misfit leading to a slightly reduced tetrahedral rotation angle (α). This brings $I - O_{outer}$ closer to $I - O_{inner}$ providing Ba^{2+} with a more highly coordinated site to distribute its charge.

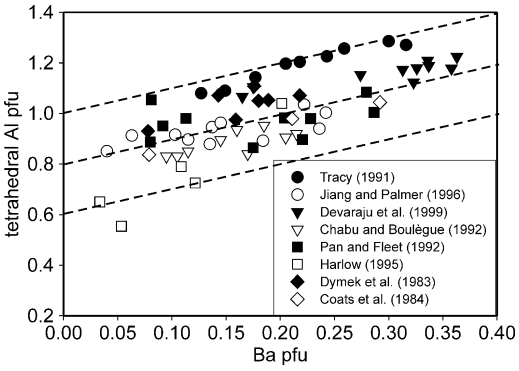

Fig. 9 Tetrahedral Al is plotted as function of Ba pfu according to the substitution $Ba + {}^{[IV]}Al \leftrightarrow K + {}^{[IV]}Si$. The data are from various rock types. The erroneous formulae presented by COATS et al. (1984) were recalculated based on their wt% analytical results. The dashed lines represent various degrees of phengite substitution. Only the data of TRACY (1991) lack a significant phengite substitution. Notice that Ba-bearing muscovites from the Simplon area (this paper) are displayed in a corresponding diagram (Fig. 2).

Acknowledgement

The authors are grateful to G.E. Harlow (New York) and R.J. Swope (Indianapolis) for their constructive reviews. R. Gieré is thanked for handling the manuscript as SMPM Editor.

References

ANKINOVICH, S.G., ANKINOVICH, E.A., ROZHDESTVENSKAYA, I.V. and FRANK-KAMENETSKII, V.A. (1972): Chernykhite, a new barium-vanadium mica from northwestern Karatau. Zap. Vses. Mineral. Obshch., 101, 451–458 (in Russian).

BAILEY, S.W. (1984): Crystal chemistry of the true micas. Reviews in Mineralogy, Micas, 13, 13–60.

BRIGATTI, M.F. and POPPI, L. (1993): Crystal chemistry of Ba-rich trioctahedral micas-1*M*. Eur. J. Mineral., 5, 857–871.

BRIGATTI, M.F., FRIGIERI, P. and POPPI, L. (1998): Crystal chemistry of Mg-, Fe-bearing muscovites-2M_1. Am. Mineral., 83, 775–785.

CHABU, M. and BOULÈGUE, J. (1992): Barian feldspars and muscovite from the Kipushi Zn–Pb–Cu deposit, Shaba, Zaire. Can. Mineral., 30, 1143–1152.

COATS, J.S., FORTEY, N.J., GALLAGHER, M.J. and GROUT, A. (1984): Stratiform barium enrichment in the Dalradian of Scotland. Econ. Geol., 79, 1585–1595.

COMODI, P. and ZANAZZI, P.F. (1997): Pressure dependence of structural parameters of paragonite. Phys. Chem. Miner., 24, 274– 280.

DEVARAJU, T.C., RAITH, M.M. and SPIERING, B. (1999): Mineralogy of the Archean barite deposit of Ghattihosahalli, Karnataka, India. Can. Mineral. 37, 603–617.

DYMEK, R.F., BOAK, J.L. and KERR, M.T. (1983): Green micas in the Archean Isua and Malene supracrustal rocks, southern West Greenland, and the occurrence of barian-chromian muscovite. Rapp. Grønlands Geol. Unders., 112, 71–82.

ENRAF NONIUS (1983): Structure determination package (SDP). Enraf Nonius, Delft, Holland.

EVSYUNIN, V.G., KASHAEV, A.A. and RASTSVETAEVA, R.K. (1997): Crystal structure of a new representative of Cr micas. Crystallogr. Reports, 42, 571–574.

FILUT, M.A., RULE, A.C. and BAILEY, S.W. (1985): Crystal structure refinement of anandite-2Or, a barium- and suphur-bearing trioctahedral mica. Am. Mineral., 70, 1298–1308.

FRANK, E. (1979): Celsian in leucocratic gneisses of the Berisal Complex. Central Alps, Switzerland. Schweiz. Mineral. Petrogr. Mitt., 59, 245–250.

GNOS, E. and ARMBRUSTER, T. (2000): Kinoshitalite, $Ba(Mg)_3(Al_2Si_2)_{10}(OH,F)_2$, a brittle mica from a manganese deposit in Oman: Paragenesis and crystal chemistry. Am. Mineral., 85, 242–250.

GUGGENHEIM, S. (1984): The brittle micas. Reviews in Mineralogy, Micas, 13, 61–104.

GUIDOTTI, C.V. (1984): Micas in metamorphic rocks. Reviews in Mineralogy, Micas, 13, 357–467.

HARLOW, G.E. (1994): Jadeitites, albitites and related rocks from the Motagua Fault Zone, Guatemala. J. Metamorphic Geol., 12, 49–68.

HARLOW, G.E. (1995): Crystal chemistry of barian enrichment in micas from metasomatized inclusions in serpentinite, Motagua Fault Zone, Guatemala. Eur. J. Mineral., 7, 775–789.

HETHERINGTON, C.J., GRAESER, S., SCHMIDT, S.T. and GIERÉ, R. (1999): Barium-bearing white mica from the Wasenalp, Simplon, Switzerland. Swiss Society of Mineralogy and Petrology. 74. Annual Meeting in Luzern, Abstracts.

HETHERINGTON, C.J., GRAESER, S., SCHMIDT, S.T. and GIERÉ, R. (2000): Barium-bearing white mica from the Wasenalp, Simplon, Switzerland. Ber. Deutsch. Mineralog. Ges., Beiheft Eur. J. Mineral., 12, 80.

JIANG, S.Y. and PALMER, M.R. (1996): Ba-rich micas from the Yindongzi-Daxigou Pb–Zn–Ag and Fe deposits, Quinling, northwestern China. Min. Mag., 60, 433–445.

LIANG, J.J., HAWTHORNE, F.C., NOVÁK, M., ČERNÝ, P. and OTTOLINI, L. (1995): Crystal-structure refinement of boromuscovite polytypes using a coupled Rietveld – static-structure energy-minimization method. Can. Mineral., 33, 859–865.

LIN, C.Y. and BAILEY, S.W. (1984): The crystal structure of paragonite-2M_1. Am. Mineral., 69, 122–127.

NI, Y. and HUGHES J.M. (1996): The crystal structure of nanpingite-2M_2, the Cs end-member of muscovite. Am. Mineral., 81, 105–110.

PAN, Y. and FLEET, M.E. (1991): Barian feldspar and barian-chromian muscovite from the Hemlo area, Ontario. Can. Mineral., 29, 481–498.

POUCHOU, J.L. and PICHOIR, F. (1984) Un nouveau modèle de calcul pour la microanalyse quantitative par spectrométrie de rayons X. La Recherche Aérospatiale, 3, 167–192.

RAASE, P., RAITH, M., ACKERMAND, D., VISWANATHA, M.N. and LAL, R.K. (1983): Mineralogy of chromiferous quartzites from South India. J. Geol. Soc. India, 24, 502–521.

ROZHDESTVENSKAYA, I.V. (1979): Refinement of the structure of chernykhite. Kristallokim. Strukt. Miner., 66–69 (in Russian).

SHANNON, R.D. (1976): Revised effective ionic radii and systematic studies of interatomic distances in halides and chalcogenides. Acta Crystallogr. A32, 751–767.

TRACY, R.J. (1991): Ba-rich micas from the Franklin Marble, Lime Crest and Sterling Hill, New Jersey. Am. Mineral., 76, 1683–1693.

SHELDRICK, G.M. (1997): SHELXL-97 and SHELXS-97. Programs for crystal structure determination. University of Göttingen, Germany.

ZHUKHLISTOV, A.P., ZVYAGIN, B.B., LAZARENKO, E.K. and PAVLISHIN, V.I. (1977): Refinement of the crystal structure of ferrous celadonite. Sov. Phys. Crystallogr., 22, 284–288.

Manuscript received March 21, 2002; revision accepted August 3, 2002.
Editorial handling: R. Gieré